

Article

Direct Growth of Flower-Shaped ZnO Nanostructures on FTO Substrate for Dye-Sensitized Solar Cells

Ahmad Umar ^{1,2,*}, Mohammad Shaheer Akhtar ³, Tubia Almas ^{1,2,4},
Ahmed Abdulbaqi Ibrahim ^{1,2}, Mohammed Sultan Al-Assiri ^{2,5}, Yoshitake Masuda ⁶ ,
Qazi Inamur Rahman ⁷ and Sotirios Baskoutas ⁴ 

¹ Department of Chemistry, Faculty of Science and Arts, Najran University, Najran 11001, Saudi Arabia

² Promising Centre for Sensors and Electronic Devices (PCSED), Najran University, Najran 11001, Saudi Arabia

³ New and Renewable Energy Material Development Center (NewREC), Chonbuk National University, Chonbuk, 54896, Korea

⁴ Department of Materials Science, University of Patras, 26504 Patras GR, Greece

⁵ Department of Physics, Faculty of Science and Arts, Najran University, Najran 11001, Saudi Arabia

⁶ National Institute of Advanced Industrial Science and Technology (AIST), 2266-98 Anagahora, Shimoshidami, Moriyama-ku, Nagoya 463-8560, Japan

⁷ Department of Chemistry, Integral University, Lucknow, Uttar Pradesh 226026, India

* Correspondence: ahmadumar786@gmail.com

Received: 27 May 2019; Accepted: 25 July 2019; Published: 4 August 2019



Abstract: The proposed work reports that ZnO nanoflowers were grown on fluorine-doped tin oxide (FTO) substrates via a solution process at low temperature. The high purity and well-crystalline behavior of ZnO nanoflowers were established by X-ray diffraction. The morphological characteristics of ZnO nanoflowers were clearly revealed that the grown flower structures were in high density with 3D floral structure comprising of small rods assembled as petals. Using UV absorption and Raman spectroscopy, the optical and structural properties of the ZnO nanoflowers were studied. The photoelectrochemical properties of the ZnO nanoflowers were studied by utilizing as a photoanode for the manufacture of dye-sensitized solar cells (DSSCs). The fabricated DSSC with ZnO nanoflowers photoanode attained reasonable overall conversion efficiency of ~1.40% and a short-circuit current density (J_{SC}) of ~4.22 mA cm⁻² with an open circuit voltage (V_{OC}) of 0.615 V and a fill factor (FF) of ~0.54. ZnO nanostructures have given rise to possible utilization as an inexpensive and efficient photoanode materials for DSSCs.

Keywords: Flower-shaped ZnO structures; FTO substrate; Dye-sensitized solar cells; Photovoltaics

1. Introduction

People need to step up efforts to find highly efficient and renewable energy sources to maintain social and economic development [1–5]. A reliable and renewable energy source, solar energy is accounted as a future energy resource due to its abundance and completely free of cost from sunlight. A low-cost wide band gap semiconducting oxide based solar cell, named dye sensitized solar cell (DSSC) is considered as potential alternative in the field of photovoltaic devices due to its high power conversion efficiency (PCE) and ease of manufacturing [6–9]. Till now, Gratzel group reported so far highest PCE of 12.3% using DSSCs with nanoporous TiO₂ photoanode [10]. Other than TiO₂ photoanode, zinc oxide (ZnO) nanomaterials are shown a great potential as an excellent wide-bandgap oxide semiconductor for photoanode in DSSCs because ZnO presents the similar band position and electron affinities along with high electron diffusivity and high electron mobility of 115 to 155 cm²V⁻¹s⁻¹, in comparison with TiO₂ [11–14]. Importantly, these special properties of ZnO are reflected to help in reduction

of recombination rate and efficient electron transport in the photoanode [15]. Most the reported DSSCs based on ZnO photoanodes are inferior to DSSCs based on the TiO₂ photoanode [16–18], which normally can be attributed to ZnO dissolution to Zn²⁺ via the adsorbed acidic dye such as N3, N719, and black dye, resulting in the aggregate formation of Zn²⁺ and dye molecules [19]. These aggregates formation of Zn²⁺/dye complexes are further blocked the injected electrons from the photoexcited dye molecules to the ZnO, which results in decrease in proper electron injection. It is realized that some extent of research on the improvement in performance of ZnO-based DSSC are needed to outperform the aggregates formation of Zn²⁺/dye complexes [19].

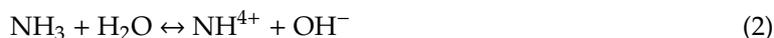
ZnO is highly scrutinized n-type semiconducting oxide owing to its an unique wide band gap of 3.37 eV and considerable large exciton binding energy of ~60 meV at ambient condition [20,21]. The unique properties of ZnO materials have attracted attention in the area of electrochemical and photoelectrochemical devices because they have special ability to grow a variety of different nanostructures [22–29]. Apart from thermal growth of ZnO, ZnO synthesis at low temperature solution processes has recently been popularized due to ease of processibility, high aspect growth ratio, low-cost, and high yield [30]. In past few years, researches are experimented to elevate the conversion efficiency of ZnO-based DSSCs by adopting different structural and morphological aspects like 1D, 2D, and 3D branched networks and mixed morphologies for preparing ZnO photoanodes [31–33]. Several works on the utilization of 1D and 2D ZnO-based photoanodes have already been reported, but the conversion efficiencies of DSSCs are not competent to TiO₂ based DSSCs [29–33].

Herein, we report the low-temperature hydrothermal synthesis, characterization, and dye-sensitized solar cell (DSSC) application of ZnO nanoflowers. The ZnO nanoflowers were grown directly on the fluorine-doped tin oxide (FTO) substrate via simple hydrothermal process and directly used as working electrode for the dye absorption in DSSCs. The manufactured DSSC poses reasonable PCE of ~1.40% along with open circuit voltage (V_{OC}) of 0.615 V, short-circuit current density (J_{SC}) of ~4.22 mA cm⁻², and a fill factor (FF) of ~0.54.

2. Materials and Methods

2.1. Synthesis of Flower-Shaped ZnO Nanostructures Directly Grown on FTO Substrate

For the growth of flower-shaped ZnO nanostructures directly on the FTO substrate, a facile hydrothermal process was adopted. Briefly, 0.05 M (1.2 g) zinc nitrate hexahydrate (Zn(NO₃)₂·6H₂O), Sigma-Aldrich, Missouri, United States) solution was mixed in 50.0 ml deionized (DI) water and stirred continuously at ambient temperature. Simultaneously, 0.05 M (0.5 g) aqueous solution of hexamethylenetetramine (HMTA, Sigma-Aldrich, Missouri, United States) was added in the stirred solution. A small portion (0.12 g) of poly(ethylene glycol) (PEG, MW: 20000, Sigma-Aldrich, Missouri, United States) was also introduced to reaction mixture under vigorous stirring at 25 °C as a binder. The pH = 8.0 was maintained by adding few drops of liquid ammonia solution. Finally, cleaned FTO substrates were horizontally placed in the Teflon beaker and the resulting mixture was poured in it [7]. The Teflon beaker was placed in the stainless steel autoclave which was heated to 150 °C for 8 h. After completion of the reaction, the ZnO coated FTO substrates were removed from the autoclave and rinsed with ethanol and DI water and dried at room temperature. Finally, the substrate was heated at 250 °C for 1 h under air condition. It was presumed that the formation of the flower-shaped morphologies on the FTO substrate follows the below mentioned chemical reactions.



Thus, ZnO nuclei were formed which after prolonged heating and reaction time, the formed ZnO nuclei were collectively assembled into the flower shaped ZnO nanostructures on the FTO substrate.

2.2. Characterizations of Flower-Shaped ZnO Nanostructures Directly Grown on FTO Substrate

Flower-shaped ZnO nanostructures directly grown on FTO substrate were examined by various techniques to inspect various characteristics and properties. The crystal structure and related characteristics were inspected by X-ray diffraction (XRD; PAN analytical Xpert Pro., Malvern Panalytical, Malvern, UK) using Cu-K α radiation ($\lambda = 1.54178 \text{ \AA}$) in the range of 20–70°. The field emission scanning electron microscopy (FESEM; JEOL-JSM-7600F, Akishima, Tokyo, Japan) was employed to monitor the morphological information of the prepared material. The qualitative localized chemical analysis and chemical compositions were inspected using energy-dispersive spectroscopy (EDS) attached with FESEM. The scattering characteristics have been investigated by Raman scattering spectroscopy (Perkin Elmer-Raman Station 400, Waltham, MA, USA) at room temperature. The X-ray Photoelectron Spectroscopy (XPS) (XPS, Kratos analytical, ESCA-3400, Shimadzu, Kyoto, Kyoto Prefecture, Japan) measurements were conducted to determine the chemical composition and the elemental states in the prepared flower-shaped ZnO nanostructures by determining the binding energies. The applied X-ray source (MgK α , 1253.6 eV) was operated at 10 kV and 20 mA. The specific Brunauer–Emmett–Teller (BET) surface area of flower-shaped ZnO nanostructures was evaluated by measuring Nitrogen adsorption via a Micromeritics ASAP 2020 nitrogen adsorption apparatus (Norcross, GA, USA).

2.3. Fabrication of ZnO Nanoparticles-Based Flower-Shaped ZnO Nanostructures Directly Grown on FTO Substrate

The DSSC based on flower-shaped ZnO nanostructures directly grown on FTO substrate was fabricated as reported earlier [7]. The flower-shaped ZnO nanostructures on FTO substrate was immersed into freshly prepared 0.3 M ethanolic solution of *cis*-bis (isothiocyanate) bis (2,2-bipyridyl-4,4-dicarboxylate)-ruthenium(II) bistetrabutyl ammonium dye (N719) for 12 h under dark condition at 298 K. Simultaneously, a counter electrode of Pt metal (thickness = 120 nm) was made by the sputtering onto the FTO substrate. To manufacture the DSSC, the dye-absorbed ZnO-based electrode was attached with Pt counter electrode and edges were sealed using a 60- μm -thick polyimide sealing sheet. Consequently, the introduction of the liquid electrolyte comprising of 0.5 M LiI, 0.05 mM I₂, and 0.2 M tert-butyl pyridine in acetonitrile was filled into cell via drilled small holes in the counter electrode. The active area of the fabricated DSSC was 0.5 cm \times 0.5 cm. For the photocurrent density-voltage (*J*-*V*) curve of the manufactured DSSC, a self-designed computerized digital multimeter coupled with ammeter and voltmeter was used under 1 sun light using the 1000 W metal halide lamp as light source. The intensity of light was adjusted and calibrated by Si reference solar cell to set the light intensity around one-sun (100 mW/cm²) at 1.5 AM. The electrochemical behavior of fabricated DSSCs was analyzed by the electrochemical impedance (EIS) measurements using VersaSTAT4 potentiostat/galvanostat. EIS plot for fabricated DSSCs was measured by applying 10 mV ac signal over the frequency range of 100 kHz to 1 Hz.

3. Results and Discussion

3.1. Characterization and Properties of Flower-Shaped ZnO Nanostructures Directly Grown on FTO Substrate

The XRD results of the synthesized ZnO nanostructures on FTO substrate are illustrated in Figure 1. From the XRD patterns, all characteristic diffraction peaks, such as (100), (002), (101), (102), (110), (103), (112), and (201), are well matched with JCPDS card no. 36-1451, deducing the hexagonal wurtzite structure of ZnO in synthesized ZnO nanostructures. Other diffraction peaks in Figure 1 are related to the FTO substrate. Moreover, the highest peak intensity at (001) for ZnO nanoflowers on the FTO substrate clearly evident that the ZnO nanoflowers grow perpendicular to the FTO substrate

surface [34–36]. Besides, no other impurity-related peak is detected from the observed XRD pattern, which revealed the wurtzite hexagonal phase of the grown nanoflowers.

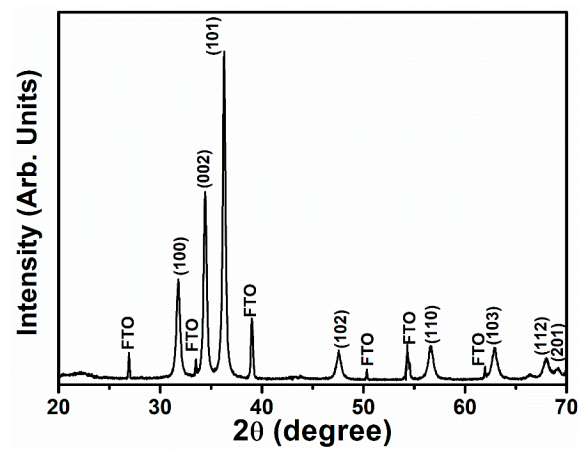


Figure 1. Typical XRD pattern of flower-shaped ZnO nanostructures directly grown on fluorine-doped tin oxide (FTO) substrate.

As shown in Figure 2a–d, the field-emission scanning electron microscopy (FESEM) images are used to explore the structure and morphology of the flower-shaped ZnO nanostructures. It is easy to see the well-grown flower-like morphology, which is comprised of small nanorods with a central peripheral rod. Figure 2c,d shows the high-resolution FESEM images of the ZnO nanostructures, which reveal that each petals are composed of agglomerated nanorods. Fascinatingly, some of the small nanorods are assembled in such a way that they are collectively formed the flower-shaped morphologies while most of the nanoflowers are grown almost perpendicularly on the surface of the substrate. These flower like morphologies are uniformly deposited on the whole substrate surface.

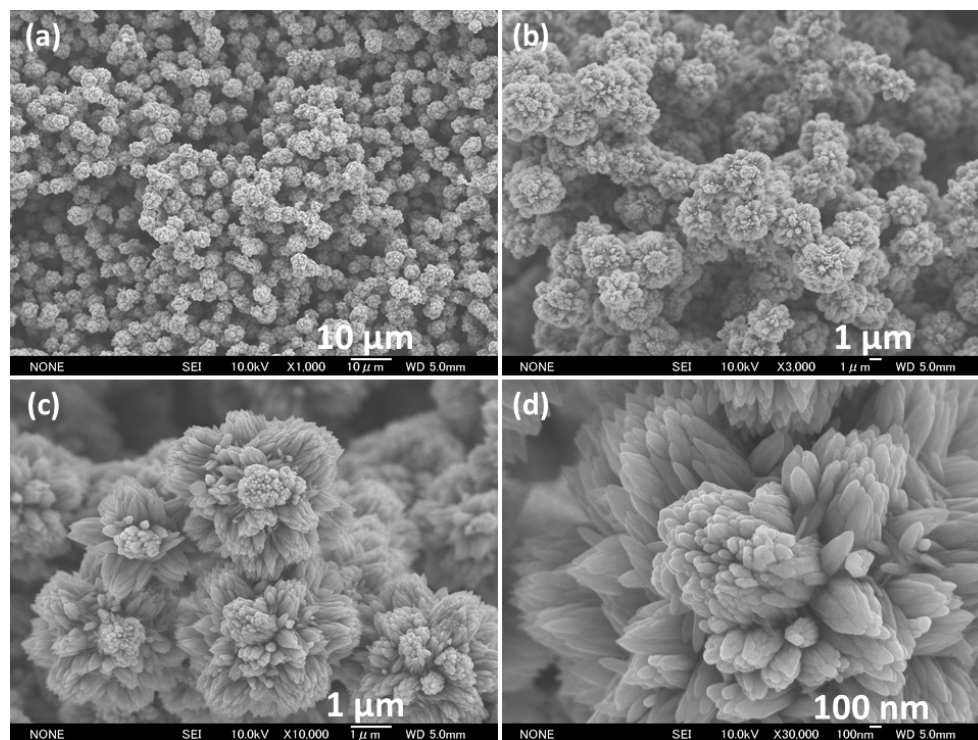


Figure 2. Typical field-emission scanning electron microscopy (FESEM) images (a–d) of flower-shaped ZnO nanostructures directly grown on FTO substrate.

Using room temperature photoluminescence (PL) spectroscopy, the optical properties of the flower-shaped ZnO nanostructures were determined, as shown in Figure 3. Before each measurement, FTO/glass was used to remove the effects of fluorine tin oxide and glass [37,38] as a reference. From Figure 3, the ZnO nanoflowers exhibits the strong emission peak at a lower wavelength along with a broad green emission at higher wavelength [39]. The ZnO nanoflowers show well-defined peak in the UV region, assigning the near-band-edge (NBE) emission of ZnO which normally appeared from the recombination process of free-exciton [40,41]. The broad green emissions are accounted from several intrinsic structural and surface defects such as interstitials oxygen defects (O_i), oxygen vacancies (V_O), and antisite oxygen (O_{Zn}) in the synthesized ZnO nanoflowers [42]. It was suggested that the emission peaks are governed the electronic transitions due to the travelling of electron from valence band to the conduction band of the ZnO nanostructures [43].

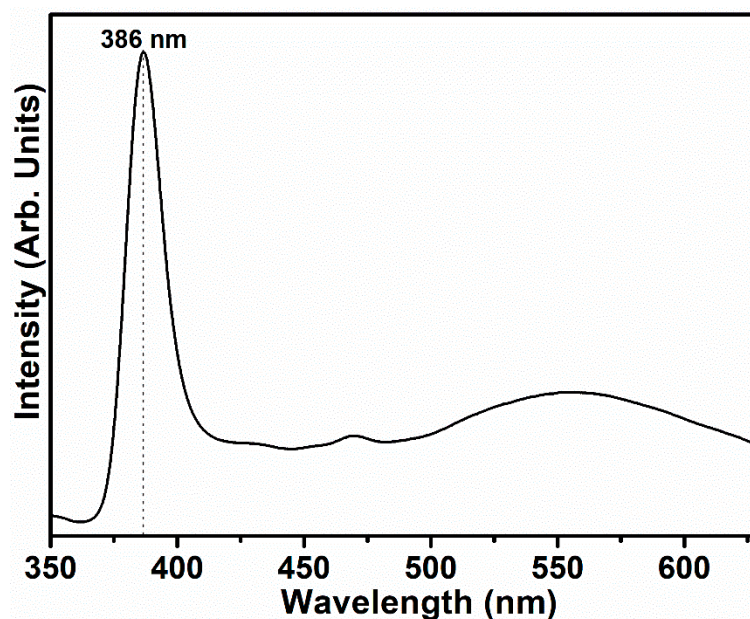


Figure 3. Room temperature PL spectrum of flower-shaped ZnO nanostructures directly grown on FTO substrate.

Raman scattering spectroscopy was determined to analyze the vibration modes and quality of the flower-shaped ZnO nanostructures, as shown in Figure 4. The intense Raman peak observed at 437.6 cm^{-1} due to metal–oxygen atom vibration, which is ascribed to E_2 (high) mode. The appeared E_2 (high) mode supports the usual formation of hexagonal ZnO nanostructures [44]. The second order Raman peak centered at 581.8 cm^{-1} is related to E_1 (LO) mode [45,46] which usually originated due to the presence of interstitials defects such as oxygen vacancies in zinc lattices. Two less intense Raman peaks centered at 335 cm^{-1} and 381 cm^{-1} are referred to E_2 (high)– E_2 (low) mode or the origin of the multiple phonon scattering processes. The intense E_2 (high) mode deduces the good crystal quality and structures of flower-shaped ZnO nanostructures grown on FTO substrate, which is well aligned with XRD outcomes.

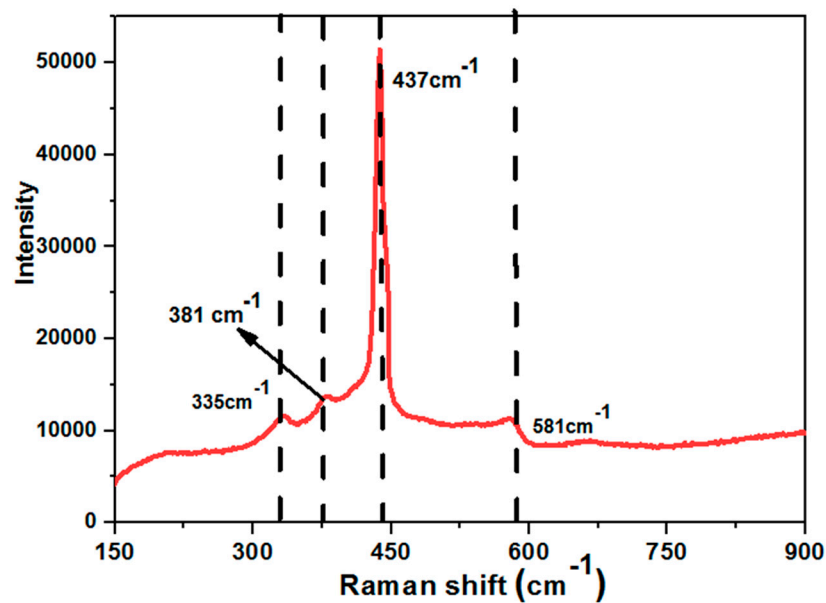


Figure 4. Typical Raman scattering spectrum of flower-shaped ZnO nanostructures directly grown on FTO substrate.

In addition, XPS measurement was evaluated for the synthesized flower-shaped ZnO nanostructures to elucidate the existence of surface species, composition, oxidation state, and electronic environment. The survey XPS (Figure 5a) spectrum displays that the synthesized ZnO nanoflowers recorded well-defined binding energies of Zn 2p, O 1s, and small C 1s. The main reason for the existence of C1s at 284 eV might be happened due to small amount of carbon species from hydrocarbons in precursors and solvents. From Figure 5b, the high-resolution Zn 2p XPS for the synthesized ZnO nanostructures shows binary binding energies at 1044.8 and 1021.7 eV, which are assigned to Zn 2p^{1/2} and Zn 2p^{3/2} spin-orbital splitting photoelectrons, respectively. Notably, the difference of Zn 2p binding energies is estimated to 23.1 eV which is evidenced for Zn²⁺ oxidation state in ZnO. From the high-resolution O 1s XPS spectra (Figure 5c), the binding energy at 530.8 eV is ascribed to the lattice Zn–O bond within the ZnO crystal. However, the two resolved binding energies at 530.3 and 532.7 eV arise from the surface oxygen over the ZnO surfaces, which usually come from the atmospheric humidity and oxygen deficiencies/vacancies. The obtained Zn 2p and O 1s binding energies again confirm the high quality ZnO crystals with less impurities.

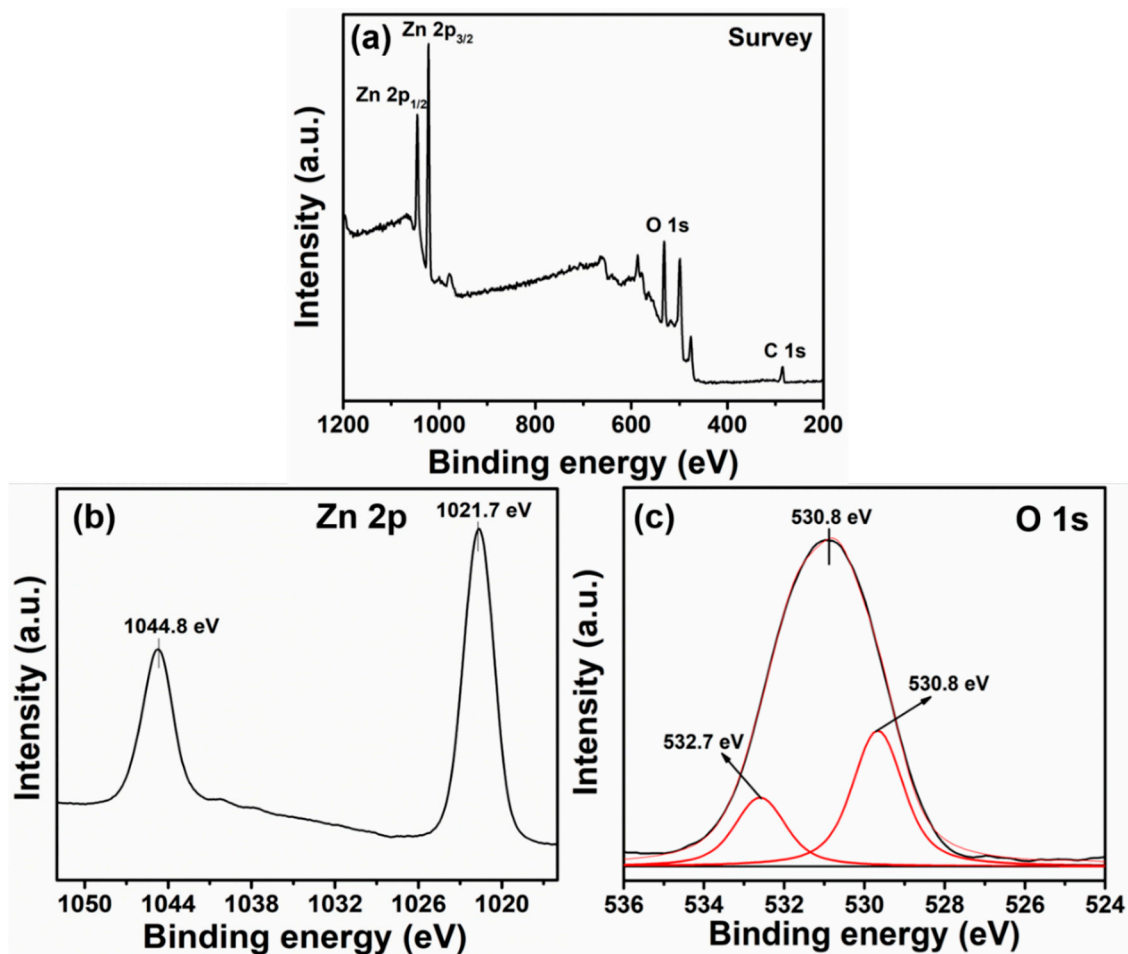


Figure 5. Typical XPS (a) full survey, (b) Zn 2p, and (c) O1s spectrum of flower-shaped ZnO nanostructures directly grown on FTO substrate.

3.2. Dye-Sensitized Solar Cell Application of Flower-Shaped ZnO Nanostructures

To define the photoelectrochemical properties of flower-shaped ZnO nanostructures, a DSSC has been manufactured and tested under 1 sun (AM1.5G, 100 mW/cm²) to assess the photovoltaic properties of the synthesized flower-shaped ZnO nanostructures based photoanode. Figure 6a shows the J–V curve of the manufactured DSSC with the synthesized flower-shaped ZnO nanostructures based photoanode. The manufactured DSSC attained the healthy overall conversion efficiency of ~1.40% along with open circuit voltage (V_{OC}) of 0.615 V, short-circuit current density (J_{SC}) of ~4.22 mA cm⁻², and a fill factor (FF) of ~0.54. Relatively good V_{OC} and FF in DSSC might be accounted from the creation of large grain sizes in the ZnO nanostructures which result in the interface recombination rate at the interface of the ZnO nanostructures/electrolyte.

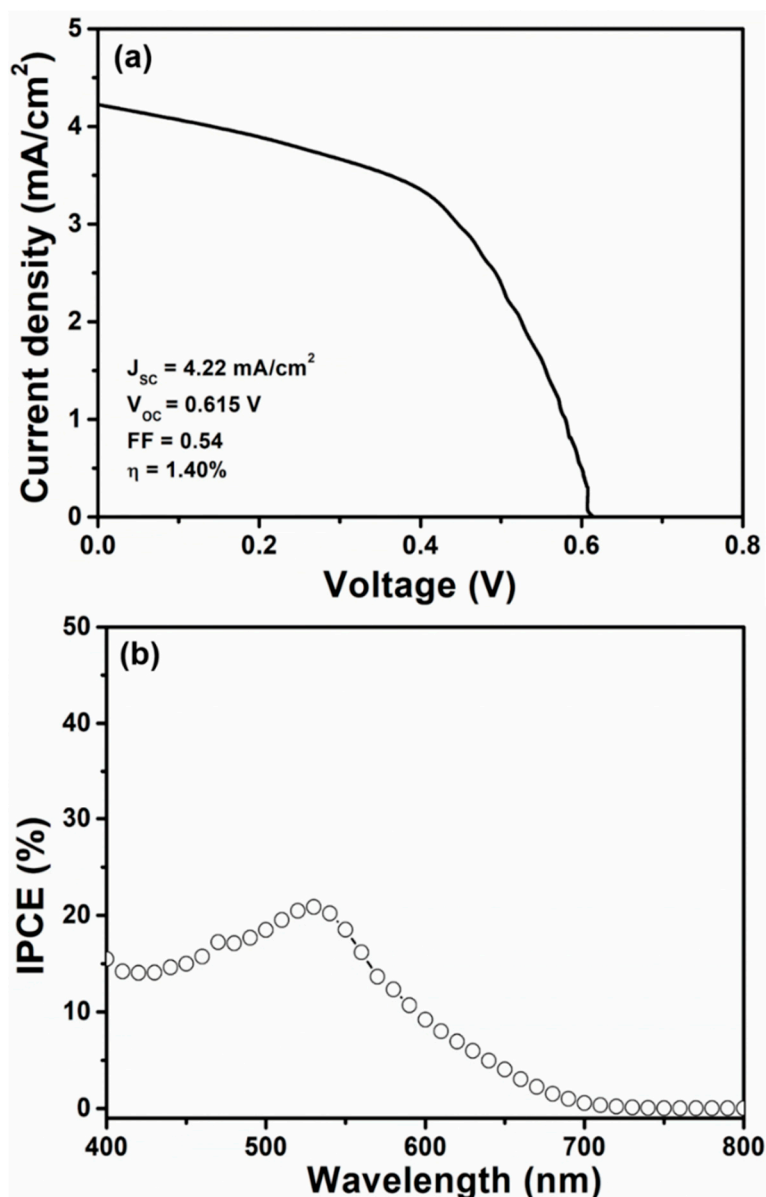


Figure 6. Typical (a) current density-voltage (J - V) characteristics and (b) incident photon-to-current conversion efficiency (IPCE) curve of manufactured dye-sensitized solar cells (DSSCs) with flower-shaped ZnO nanostructures based photoanode.

The low efficiency and J_{sc} in manufactured DSSC with flower-shaped ZnO nanostructures based photoanode are attributed to its nonuniform distribution of flowers and low specific surface area (Surface area = 8.351 m²/g), resulting in moderate amount of dye absorption via the flower-shaped ZnO nanostructure based photoanode. The yielded photovoltaic parameters of manufactured DSSC are better than those of similarly DSSCs fabricated with ZnO-based photoanode [47–52]. Moreover, the low J_{sc} of manufactured DSSC was affiliated to the low surface area and low efficiency of light harvesting. In order to elucidate the light harvesting and photocurrent, an incident photon to current efficiency (IPCE) analysis of the manufactured DSSC with synthesized flower-shaped ZnO nanostructures based photoanode was measured as a function of wavelength. As we know, the estimation of IPCE is from the efficiencies of the processes which evaluate the solar energy to electrical conversion in DSSCs by using the below equation.

$$IPCE (\%) = \eta_{lh}(\lambda) \eta_{inj}(\lambda) \eta_{col}(\lambda) \quad (5)$$

where $\eta_{lh}(\lambda)$ is the light-harvesting efficiency, $\eta_{inj}(\lambda)$ is the electron injection efficiency from the sensitizer into the semiconductor oxide layer, and $\eta_{col}(\lambda)$ is the electron collection efficiency. Figure 6b shows the IPCE curve of the manufactured DSSC with the synthesized flower-shaped ZnO nanostructure-based photoanode using the range of a wavelength range from 400 to 800 nm. The maximum IPCE of ~21% at 530 nm for the manufactured DSSC is attained, and also estimates the integrated J_{SC} value of ~4.67 mA/cm² from the obtained IPCE result. It is visible that the integrated J_{SC} value is in well-aligned with the J_{SC} value extracted from the J–V curve. The low IPCE value is also associated to the poor light harvesting efficiency in dye absorbed flower-shaped ZnO nanostructures based photoanode. Further, the flower-shaped ZnO nanostructures are assumed to have a poor surface for dye absorption, contributing to the high recombination of electrons and relatively low injection rate of electrons. These factors might have restricted to achieve high performance and photocurrent density in DSSC using flower-shaped ZnO nanostructures based photoanode. Table 1 exhibits the photovoltaic performance of variety of fabricated DSSCs based on the utilization of different ZnO nanostructures as photoanodes [47–59].

Table 1. Photovoltaic performance of fabricated DSSCs based on different ZnO nanostructure-based photoanodes.

Morphologies of ZnO Nanostructures	Substrate	Dye	Photovoltaic Performances				Ref.
			J_{SC} (mA/cm ²)	V_{OC} (V)	FF	η (%)	
Nanoparticles	FTO	N719	5.4	0.58	0.35	1.1	47
Tripods	FTO	N719	2.80	0.55	0.54	0.88	48
Bush-like morphology	FTO	N719	3.46	0.69	0.35	0.82	49
Nanorods	FTO	N3	1.37	0.845	0.69	0.80	50
Aligned nanorods	FTO	N719	2.08	0.736	0.43	0.66	51
Paddle wheel like structured ZnO nanorod	FTO	-	2.82	0.70	0.65	1.3	52
ZnO nanorods	FTO	N719	1.69–2.13	-	-	0.36–0.47	53
ZnO nanorods	FTO	N719	1.52	0.361	0.37	0.21	54
Nanorods + nanosheets	Zn foil	N719	3.041	0.524	0.42	0.67	55
Nanotubes	ITO	N3	4.70	0.386	-	1.20	56
Nanograsses	FTO	N719	1.93	0.630	0.39	0.47	57
Nanocombs	FTO	N719	3.14	0.671	0.34	0.68	58
Nanofibers	FTO	N719	2.87	0.690	0.44	0.88	59
ZnO nanoflowers directly grown on FTO	FTO	N719	4.22	0.615	0.54	1.40	This work

Electrochemical impedance spectroscopy (EIS) for DSSCs with flower-shaped ZnO nanostructures has been performed to explain the charge transport and recombination mechanisms. Figure 7 illustrates the typical Nyquist plot along with equivalent circuit for the fabricated DSSC with flower-shaped ZnO nanostructure-based photoanode. Generally, the Nyquist plot comprises of three semicircles with respect to frequency, which are associated with charge transfer within the electrolyte (R_S), charge transfer at electrolyte/counter electrode interface (R_{CE}), and electron transfer at the electrolyte/semiconductor oxide interface (R_{CT}) [60], as shown Figure 7. Fabricated DSSC presents the large R_{CT} of 142 Ω and large R_S of 73.5 Ω (as estimated from Figure 7), suggesting the lesser charge transfer at the interface of dye-loaded ZnO and electrolyte layer. In this work, R_{CT} and R_S values are higher than that of DSSCs fabricated based on ZnO nanoparticles (low R_S and low R_{CT}), which clearly indicates weak charge transportation at ZnO/electrolyte interface [61]. It is believed that the high R_{CT} and R_S values obtained by DSSCs with flower-shaped ZnO nanostructure-based photoanode clearly explains the unfavorable electron transport, thus it probably leads to fast electron recombination rate. This result is also consistent with low photovoltaic parameters for DSSCs with flower-shaped ZnO nanostructure-based photoanode.

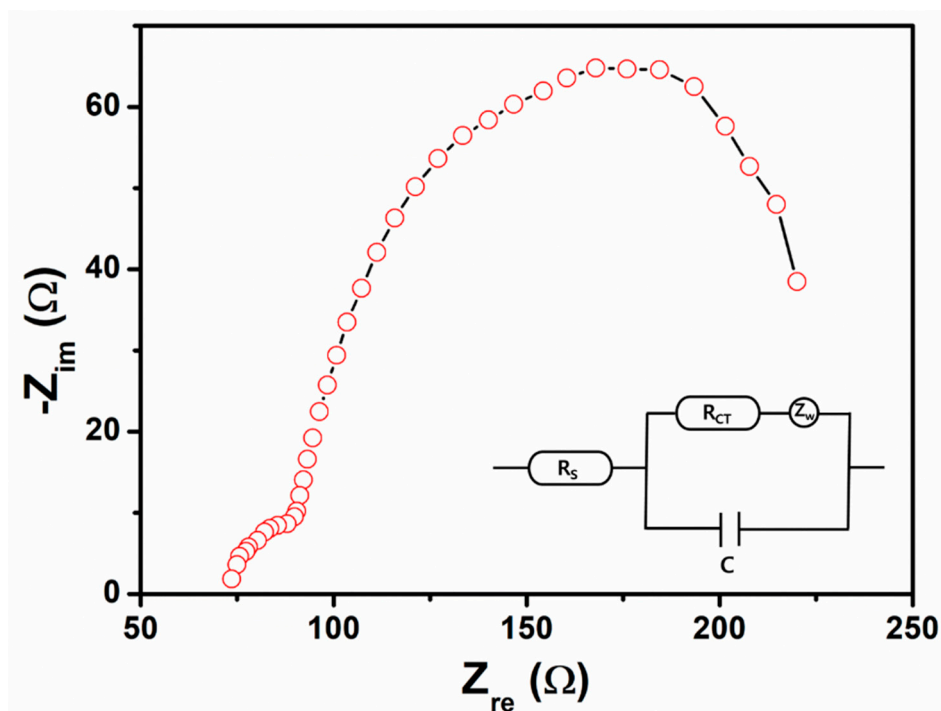


Figure 7. Nyquist plot of fabricated DSSC with flower-shaped ZnO nanostructure-based photoanode and inset shows equivalent circuit of fabricated device.

4. Conclusions

In summary, using a simple solution process at low temperature, the flower-shaped ZnO nanostructures with high crystallinity were directly synthesized on FTO substrate and successfully applied as photoanodes for the manufacturing of DSSC. It was found that the petals in flower morphology were comprised of aggregated small rods with high aspect ratio. XPS studies were confirmed that highly pure ZnO made up of Zn^{2+} and O^{2-} states. The optical and structural characterizations were deduced the excellent crystal quality with lesser defect in the synthesized flower-shaped ZnO nanostructures. As a photoanode, the manufactured DSSC recorded reasonable overall conversion efficiency of $\sim 1.40\%$ with good J_{SC} and V_{OC} . From IPCE curve, the integrated J_{SC} of $\sim 4.67 \text{ mA/cm}^2$ is similar to J_{SC} value extracted from J-V curve. It is confirmed from this study that the reported route of synthesis is an easy method for preparing high quality ZnO crystal with flower-like morphology, which has excellent prospects in photoelectrochemical applications.

Author Contributions: A.U., M.S.A., T.A., A.A.I. and S.B. conceived and designed the experiments; A.U., M.S.A., T.A., A.A.I., Y.M. and Q.I.R. performed the experiments and characterized the samples, A.U., M.S.A., T.A., A.A.I., M.S., A.Y.M. and Q.I.R. analyzed the data contributed reagents/materials/analysis tools and wrote the paper.

Funding: This work was funded by the Deanship of Scientific Research (DSR), Najran University, Najran, under grant no. NU/ESCI/16/016.

Acknowledgments: The authors, therefore, greatly acknowledge with thanks DSR, Najran University for technical and financial support.

Conflicts of Interest: The authors declare no conflicts of interest.

References

- Xu, F.; Sun, L. Solution-derived ZnO nanostructures for photoanodes of dye-sensitized solar cells. *Energy Environ. Sci.* **2011**, *4*, 818. [[CrossRef](#)]
- Zhang, T.; Yang, W.; Yang, Q.; Yang, P.; Sun, W. Cost-Efficient Chemical Bath Synthesized Alloy Catalysts $PtM_{0.05}$ ($M = Fe, Co, Ni$) Acting as Counter Electrodes for CdS Quantum Dot Sensitized Solar Cell. *Sci. Adv. Mater.* **2018**, *10*, 1489–1497. [[CrossRef](#)]

3. Heo, J.H.; Lee, M.H.; Song, D.H.; Aung, N.M.S.; Lee, J.J.; Song, C.E.; Hong, K.H.; Im, S.H. Highly Stable All-Inorganic Pb-Free Perovskite Solar Cells. *J. Nanoelectron. Optoelectron.* **2018**, *13*, 1764–1768. [[CrossRef](#)]
4. Ni, S.; Guo, F.; Wang, D.; Jiao, S.; Wang, J.; Zhang, Y.; Wang, B.; Feng, P.; Zhao, L. Modification of TiO₂ Nanowire Arrays with Sn Doping as Photoanode for Highly Efficient Dye-Sensitized Solar Cells. *Crystals* **2019**, *9*, 113. [[CrossRef](#)]
5. Patil, V.; Patil, A.; Yoon, S.J.; Choi, J.W. Electrochemical Characterization of Si/Al Multilayer Thin Film Anode Materials for High Energy Lithium Secondary Batteries. *Sci. Adv. Mater.* **2018**, *10*, 507–512. [[CrossRef](#)]
6. Gleiter, H. Nanostructured materials: Basic concepts and microstructure. *Acta Mater.* **2018**, *48*, 1–29. [[CrossRef](#)]
7. Umar, A.; Singh, P.; Al-Ghamdi, A.A.; Al-Heniti, S. Direct Growth of ZnO Nanosheets on FTO Substrate for Dye-Sensitized Solar Cells Applications. *J. Nanosci. Nanotech.* **2010**, *10*, 6666–6671. [[CrossRef](#)]
8. Cho, D.H.; Lee, W.J.; Wi, J.H.; Yu, H.J.; Han, W.S.; Chung, Y.D. Engineering of Sodium Supply into Cu(In,Ga)Se₂ Thin-Film Solar Cells. *J. Nanoelectron. Optoelectron.* **2018**, *13*, 1753–1757. [[CrossRef](#)]
9. Cao, V.M.H.; Hwang, S.H.; Lin, J.; Lee, S.H.; Kim, S.; Lee, J. Effects of Photosintering on Properties of Cadmium Sulfide Thin Films for Highly Efficient Cu(In, Ga)(Se, S)₂ Solar Cells. *Sci. Adv. Mater.* **2018**, *10*, 1133–1139. [[CrossRef](#)]
10. Yella, A.; Lee, H.W.; Tsao, H.N.; Yi, C.; Chandiran, A.K.; Nazeeruddin, M.K.; Diao, E.W.G.; Yeh, C.Y.; Zakeeruddin, S.M.; Gratzel, M. Porphyrin-sensitized solar cells with cobalt (II/III)-based redox electrolyte exceed 12 percent efficiency. *Science* **2011**, *334*, 629–634. [[CrossRef](#)]
11. Akhtar, M.S.; Ameen, S.; Jung, I.S.; Choi, J. Facile Synthesis of Hexagonal ZnO Nanorods for Dye-Sensitized Solar Cell Application. *J. Nanoelectron. Optoelectron.* **2018**, *13*, 1912–1916. [[CrossRef](#)]
12. Yu, W.C.; Sabastian, N.; Chang, W.C.; Tsia, C.Y.; Lin, C.M. Electrochemical Deposition of ZnO Porous Nanoplate Network for Dye-Sensitized Solar Cells. *J. Nanosci. Nanotechnol.* **2018**, *18*, 56–61. [[CrossRef](#)] [[PubMed](#)]
13. Al-Hajry, A.; Umar, A.; Hahn, Y.B.; Kim, D.H. Growth, properties and dye-sensitized solar cells applications of ZnO nanorods grown by low-temperature solution process. *Superlattices Microstruct.* **2009**, *45*, 529–534. [[CrossRef](#)]
14. Jang, J.S.; Kim, J.; Suryawanshi, M.P.; Lokhande, A.C.; Shin, H.H.; Lee, D.S.; Kim, J.H. Effect of Radio Frequency Power on the Properties of Al-Doped ZnO (AZO) Thin Films and Their Application to Cu₂ZnSn(S,Se)₄ Thin-Film Solar Cells. *J. Nanoelectron. Optoelectron.* **2018**, *13*, 1689–1694. [[CrossRef](#)]
15. Vittala, R.; Ho, K.C. Zinc oxide based dye-sensitized solar cells: A review. *Renew. Sustain. Energy Rev.* **2017**, *70*, 920–935. [[CrossRef](#)]
16. Sacco, A.; Lamberti, A.; Gazia, R.; Bianco, S.; Manfredi, D.; Shahzad, N.; Cappelluti, F.; Mac, S.; Tresso, E. High efficiency dye-sensitized solar cells exploiting spongelike ZnO nanostructures. *Phys. Chem. Chem. Phys.* **2012**, *14*, 16203–16208. [[CrossRef](#)] [[PubMed](#)]
17. Cheng, C.; Shi, Y.; Zhu, C.; Li, W.; Wang, L.; Fung, K.K.; Wang, N. ZnO hierarchical structures for efficient quasi-solid dye-sensitized solar cells. *Phys. Chem. Chem. Phys.* **2011**, *13*, 10631–10634. [[CrossRef](#)]
18. Pugliese, D.; Bella, F.; Cauda, V.; Lamberti, A.; Sacco, A.; Tresso, E.; Bianco, S. A chemometric approach for the sensitization procedure of ZnO flowerlike microstructures for dye-sensitized solar cells. *ACS Appl. Mater. Interfaces* **2013**, *5*, 11288–11295. [[CrossRef](#)]
19. Parks, G.A. The isoelectric points of solid oxides, solid hydroxides, and aqueous hydroxo complex systems. *Chem. Rev.* **1965**, *65*, 177–198. [[CrossRef](#)]
20. Chandrakala, V.; Steffy, J.A.J.; Bachan, N.; Jeyarani, W.J.; Tenkyong, T.; Shyla, J.M. A Comparative Investigation of Dye-Sensitized Titanium Dioxide (TiO₂) Nanorods Grown on Indium Tin Oxide (ITO) Substrates by Direct and Seed-Mediated Hydrothermal Methods. *Acta Metallurgica Sinica Engl. Lett.* **2016**, *29*, 457–463. [[CrossRef](#)]
21. Meyer, B.K.; Alves, H.; Hofmann, D.M.; Kriegseis, W.; Forster, D.; Bertram, F.; Christen, J.; Hoffmann, A.; Straburg, M.; Dworzak, M.; et al. Bound exciton and donor-acceptor pair recombinations in ZnO. *Phys. Status Solidi Basic Res.* **2004**, *241*, 231–260. [[CrossRef](#)]
22. Yang, J.; Yi, W.; Zhang, L.; Li, T.; Chao, Z.; Fan, J. Facile Fabrication of ZnO Nanomaterials and Their Photocatalytic Activity Study. *Sci. Adv. Mater.* **2018**, *10*, 1721–1728. [[CrossRef](#)]
23. Talib, R.A.; Ahmed, N.M.; Mohammad, S.M.; Abdullah, M.J.; Bououdina, M. ZnO Nanorods/Polyaniline Heterojunction onto SiO₂ for Photosensor. *J. Nanoelectron. Optoelectron.* **2018**, *13*, 1034–1040. [[CrossRef](#)]

24. Hassan, N.K.; Hashim, M.R.; Allam, N.K. ZnO nano-tetrapod photoanodes for enhanced solar-driven water splitting. *Chem. Phys. Lett.* **2012**, *549*, 62–66. [[CrossRef](#)]
25. Nam, G.; Leem, J.Y. Cadmium Chloride-Assisted ZnO Nanorod Regrowth for Enhanced Photoluminescence and Ultraviolet Sensing Properties. *Sci. Adv. Mater.* **2018**, *10*, 397–400. [[CrossRef](#)]
26. Tan, W.K.; Muto, H.; Ito, T.; Kawamura, G.; Lockman, Z.; Matsuda, A. Facile Fabrication of Plasmonic Enhanced Noble-Metal-Decorated ZnO Nanowire Arrays for Dye-Sensitized Solar Cells. *J. Nanosci. Nanotechnol.* **2020**, *20*, 359–366.
27. Wang, Z.H.; Yang, C.C.; Yu, H.C.; Peng, Y.M.; Su, Y.K. Electron Emission Enhanced Properties of Gold Nanoparticle-Decorated ZnO Nanosheets Grown at Room Temperature. *Sci. Adv. Mater.* **2018**, *10*, 1675–1679. [[CrossRef](#)]
28. Özgür, Ü.; Alivov, Y.I.; Liu, C.; Teke, A.; Reshchikov, M.A.; Doğan, S.; Avrutin, V.; Cho, S.J.; Morkoc, H. A comprehensive review of ZnO materials and devices. *J. Appl. Phys.* **2005**, *98*, 1–103. [[CrossRef](#)]
29. Kim, E.B.; Lee, J.E.; Akhtar, M.S.; Ameen, S.; Fijahi, L.; Seo, H.K.; Shin, H.S. Electrical Sensor Based on Hollow ZnO Spheres for Hydrazine Detection. *J. Nanoelectron. Optoelectron.* **2018**, *13*, 1769–1776. [[CrossRef](#)]
30. Ameen, S.; Akhtar, M.S.; Kim, Y.S.; Yang, O.-B.; Shin, H.-S. Influence of seed layer treatment on low temperature grown ZnO nanotubes: Performances in dye sensitized solar cells. *Electrochim. Acta* **2011**, *56*, 1111–1116. [[CrossRef](#)]
31. Park, H.; Alhamadi, S.; Bouras, K.; Schmerber, G.; Ferblantier, G.; Dinia, A.; Slaoui, A.; Jeon, C.W.; Park, C.; Kim, W.K. Nd-Doped SnO₂ and ZnO for Application in Cu(InGa)Se₂ Solar Cells. *Sci. Adv. Mater.* **2017**, *9*, 2114–2120. [[CrossRef](#)]
32. Akhtar, M.S.; Cheralathan, K.K.; Chun, J.M.; Yang, O.B. Composite electrolyte of heteropolyacid (HPA) and polyethylene oxide (PEO) for solid-state dye-sensitized solar cell. *Electrochim. Acta* **2008**, *53*, 6623. [[CrossRef](#)]
33. Galoppini, E.; Rochford, J.; Chen, H.; Saraf, G.; Lu, Y.; Hagfeldt, A.; Boschloo, G. Fast Electron Transport in Metal Organic Vapor Deposition Grown Dye-sensitized ZnO Nanorod Solar Cells. *J. Phys. Chem. B* **2006**, *110*, 16159. [[CrossRef](#)] [[PubMed](#)]
34. Chen, H.M.; Chen, C.K.; Liu, R.-S.; Zhang, L.; Zhang, J.; Wilkinson, D.P. Nano-architecture and material designs for water splitting photoelectrodes. *Chem. Soc. Rev.* **2012**, *41*, 5654–5671. [[CrossRef](#)] [[PubMed](#)]
35. Kaur, M.; Umar, A.; Mehta, S.K.; Singh, S.; Kansal, S.K.; Fouad, H.; Alothman, O.Y. Rapid solar-light driven photocatalytic degradation of methylene blue using MoS₂-ZnO heterostructure nanorods photocatalyst. *Materials* **2018**, *11*, 2254.
36. Kumar, R.; Umar, A.; Rana, D.S.; Sharma, P.; Chauhan, M.S.; Chauhan, S. Fe-doped ZnO nanoellipsoids for enhanced photocatalytic and highly sensitive and selective picric acid sensor. *Mater. Res. Bull.* **2018**, *102*, 282–288. [[CrossRef](#)]
37. Marimuthu, T.; Anandhan, N. Effect of polyvinyl alcohol on electrochemically deposited ZnO thin films for DSSC applications. *AIP Conf. Proc.* **2017**, *1832*, 080014.
38. Özdamar, T.; Taktakoglu, R.; Özdamar, H.; Esen, M.; Takçi, D.K.; Kavak, H. Crystallinity improvement of ZnO nanorods by optimization of low-cost electrodeposition technique. *Thin Solid Films* **2015**, *592 Pt A*, 143–149. [[CrossRef](#)]
39. Umar, A.; Hahn, Y.B. Ultraviolet-Emitting ZnO Nanostructures on Steel Alloy Substrate: Growth and Properties. *Cryst. Growth Des.* **2008**, *8*, 2741–2747. [[CrossRef](#)]
40. Umar, A.; Kim, S.H.; Karunakaran, B.; Suh, E.-K.; Hahn, Y.B. Growth and optical properties of aligned hexagonal ZnO nanoprisms on silicon substrate by non-catalytic thermal evaporation. *Inorg. Chem.* **2008**, *47*, 4088–4094. [[CrossRef](#)]
41. Umar, A.; Kim, S.H.; Suh, E.-K.; Hahn, Y.B. Ultraviolet-emitting javelin-like ZnO nanorods by thermal evaporation: Growth mechanism, structural and optical properties. *Chem. Phys. Lett.* **2007**, *440*, 110–115. [[CrossRef](#)]
42. Umar, A.; Ribeiro, C.; Al-Hajry, A.; Masuda, Y.; Hahn, Y.B. Growth of highly c-axis oriented ZnO nanorods on ZnO/Glass substrate: Growth mechanism, Structural and Optical properties. *J. Phys. Chem. C* **2009**, *113*, 14715–14720. [[CrossRef](#)]
43. Madlol, R.A.A. Structural and optical properties of ZnO nanotube synthesis via novel method. *Results Phys.* **2017**, *7*, 1498–1503. [[CrossRef](#)]
44. Yang, J.; Wang, Y.; Kong, J.; Jia, H.; Wang, Z. Synthesis of ZnO nanosheets via electrodeposition method and their optical properties, growth mechanism. *Opt. Mater.* **2015**, *46*, 179–185. [[CrossRef](#)]

45. Ameen, S.; Akhtar, M.S.; Shin, H.-S. Speedy photocatalytic degradation of bromophenol dye over ZnO nanoflowers. *Mater. Lett.* **2017**, *209*, 150–154. [[CrossRef](#)]
46. Marimuthu, T.; Anandhan, N.; Thangamuthu, R.; Surya, S. Facile growth of ZnO nanowire arrays and nanoneedle arrays with flower structure on ZnO-TiO₂ seed layer for DSSC applications. *J. Alloys Compd.* **2017**, *693*, 1011–1019. [[CrossRef](#)]
47. Patwari, J.; Shyamal, S.; Khan, T.; Ghadi, H.; Bhattacharya, S.; Chakrabarti, S.; Pal, S.K. Inversion of activity in DSSC for TiO₂ and ZnO photo-anodes depending on the choice of sensitizer and carrier dynamics. *J. Luminescence* **2019**, *207*, 169–176. [[CrossRef](#)]
48. Bahadur, L.; Kushwaha, S. Structural and optical properties of tripod-like ZnO thin film and its application in dye-sensitized solar cell. *J. Solid State Electron.* **2013**, *17*, 2001–2008. [[CrossRef](#)]
49. Qin, Z.; Huang, Y.; Qi, J.; Li, H.; Su, J.; Zhang, Z. Facile synthesis and photoelectrochemical performance of the bush-like ZnO nanosheets film. *Solid State Sci.* **2012**, *14*, 155–158. [[CrossRef](#)]
50. Rajan, A.K.; Cindrella, L. Ameliorating the photovoltaic conversion efficiency of ZnO nanorod based dye-sensitized solar cells by strontium doping. *Superlatt. Microstruc.* **2019**, *128*, 14–22. [[CrossRef](#)]
51. Dou, Y.; Wu, F.; Mao, C.; Fang, L.; Guo, S.; Zhou, M. Enhanced photovoltaic performance of ZnO nanorod-based dye-sensitized solar cells by using Ga doped ZnO seed layer. *J. Alloys Compd.* **2015**, *633*, 408–414. [[CrossRef](#)]
52. Senthil, T.S.; Muthukumarasamy, N.; Kang, M. Applications of highly ordered paddle wheel like structured ZnO nanorods in dye sensitized solar cells. *Mater. Lett.* **2013**, *102–103*, 26–29. [[CrossRef](#)]
53. Cai, F.; Wang, J.; Yuan, Z.; Duan, Y. Magnetic-field effect on dye-sensitized ZnO nanorods-based solar cells. *J. Power Sour.* **2012**, *216*, 269–272. [[CrossRef](#)]
54. Gonzalez-Valls, I.; Lira-Cantu, M. Effect of testing conditions on the photovoltaic performance of ZnO-based dye sensitized solar cells. *Phys. Procedia* **2010**, *8*, 28–32. [[CrossRef](#)]
55. Zhu, S.; Shan, L.; Tian, X.; Zheng, X.; Sun, D.; Liu, X.; Wang, L.; Zhou, Z. Hydrothermal synthesis of oriented ZnO nanorod-nanosheets hierarchical architecture on zinc foil as flexible photoanodes for dye-sensitized solar cells. *Ceram. Int.* **2014**, *40*, 11663–11670. [[CrossRef](#)]
56. Liu, Z.; Liu, C.; Ya, J.; Lei, E. Controlled synthesis of ZnO and TiO₂ nanotubes by chemical method and their application in dye-sensitized solar cells. *Renew. Energy* **2011**, *36*, 1177–1181. [[CrossRef](#)]
57. Zhu, S.; Chen, X.; Zuo, F.; Jiang, M.; Zhou, Z.; Hui, D. Controllable synthesis of ZnO nanograss with different morphologies and enhanced performance in dye-sensitized solar cells. *J. Solid State Chem.* **2013**, *197*, 69–74. [[CrossRef](#)]
58. Umar, A. Growth of comb-like ZnO nanostructures for Dye-sensitized solar cells applications. *Nanoscale Res. Lett.* **2009**, *4*, 1004–1008. [[CrossRef](#)]
59. Li, S.; Zhang, X.; Jiao, X.; Lin, H. One-step large-scale synthesis of porous ZnO nanofibers and their application in dye-sensitized solar cells. *Mater. Lett.* **2011**, *65*, 2975–2978. [[CrossRef](#)]
60. Wang, Z.S.; Kawauchi, H.; Kashima, T.; Arakawa, H. Significant influence of TiO₂ photoelectrode morphology on the energy conversion efficiency of N719 dye-sensitized solar cell. *Coord. Chem. Rev.* **2004**, *248*, 1381–1389. [[CrossRef](#)]
61. Golsheikh, A.M.; Kamali, K.Z.; Huang, N.M.; Zak, A.K. Effect of calcination temperature on performance of ZnO nanoparticles for dye-sensitized solar cells. *Powder Technol.* **2018**, *329*, 282–287. [[CrossRef](#)]

